


Cite this: *Nanoscale Adv.*, 2024, 6, 1122

Light-driven nanomotors with reciprocating motion and high controllability based on interference techniques†

Mohammadbagher Mohammadnezhad,^a Salah Raza Saeed,^{bd}
Sarkew Salah Abdulkareem^c and Abdollah Hassanzadeh ^{*a}

In this paper, we investigate the controlled movement of optically trapped nano-particles in an interference optical lattice. The suggested interferometric optical tweezers setup utilizes the superposition of three orthogonal Gaussian standing waves to create 3D optical lattices. Dynamic control over the constructed lattices can be achieved simply by changing the incident beam parameters using a polarizer or a phase shifter. The trapping properties of the generated optical lattices for a dielectric Rayleigh particle are numerically evaluated using a MATLAB program. The simulation results showed that the generated lattices can be translated by altering the relative phase between the interfering beams. More complex transformations and geometries can be achieved by changing other properties of the interfering beams such as the polarization state. This simple setup enables the construction of a rich variety of dynamic optical lattices and offers promising applications in colloidal and biological science such as controlling the diffusion of colloidal particles and stretching or compressing tethered polymeric molecules. This interferometric method can also be used in light-driven nanomotors with high controllability.

Received 23rd August 2023
Accepted 29th December 2023

DOI: 10.1039/d3na00678f

rsc.li/nanoscale-advances

Introduction

A nanomotor is a nanoscale energy transducer that converts diverse forms of energy into useful mechanical work.¹ Nanomotors have shown great promise for many biomedical and environmental applications.^{1,2} Different propulsion mechanisms have been proposed and used to power nanomotors. For example, nanomotors can be propelled by electric fields,³ magnetic fields,⁴ ultrasound⁵ or light.¹ Light-driven nanomotors have demonstrated several distinct advantages over other nanomotors, for example high spatial resolution, high controllability and programmability of light-driven nanomotors.^{2,6}

The external degrees of freedom of microscopic particles can be controlled by using the mechanical action of light which is known as optical manipulation or optical trapping. This technique has received great attention due to advantages such as the contactless nature of the optical forces.⁷ Most tweezers systems exploit the optical force produced by a highly focused laser

beam to confine a small particle near the beam focus.⁸ However, a single beam is capable of manipulating only one object, and to have enhanced levels of control over the microscopic world, the use of multiple-traps is necessary.⁹

One of the special types of multiple-traps with crucial importance is a periodic trapping potential which is best suitable for some specific applications, such as particle sorting,¹⁰ particle arrangement,¹¹ and creation and evolution of large arrays of colloids.¹²

There are several methods to create periodic multiple-traps, each with its own advantages and disadvantages.¹³ One of the most popular and powerful methods to create a periodic potential, an optical lattice, is the use of the interference effects of multiple coherent beams.¹⁴ One important advantage of using interference methods to produce an optical lattice is that the geometry of the lattice is under complete control.¹⁵

However, although a rich variety of different interferometric configurations were proposed and studied,^{16–18} more work is needed to take advantage of powerful features of interference approaches.

In our earlier studies, we suggested a number of different interferometric trapping setups, and their potential applications in optical manipulation were discussed.^{19–22}

A dynamic control over periodic interference traps can enhance the capabilities of such periodic patterns and pave the way to some great new applications. One way to do this is to use holographic techniques,²³ but the manipulability of holographic methods is considerably limited by the speed of the beam control.⁹

^aDepartment of Physics, University of Kurdistan, Sanandaj, Iran. E-mail: a.hassanzadeh@uok.ac.ir

^bAdvanced Polymeric Materials Research Lab., Department of Physics, College of Science, University of Sulaimani, Sulaimani, Iraq

^cDepartment of Physics, College of Science, University of Halabja, Iraq

^dDepartment of Computer Science, Cihan University, Sulaimaniya 46001, Kurdistan Region, Iraq

† Electronic supplementary information (ESI) available. See DOI: <https://doi.org/10.1039/d3na00678f>



In this paper a novel interferometric configuration to create 3D dynamic optical lattices is proposed, and its potential applications in different areas are discussed. Dynamic control over the trap positions and distances can be achieved by adjusting the polarization state or relative phase of the interfering beams.

Theory

The proposed setup exploits the interference of three pairs of mutually perpendicular counter-propagating Gaussian beams of wavelength $\lambda_0 = 632.8$ nm to create optical lattices, as schematically illustrated in Fig. 1. Dynamic control of the generated lattices can be achieved through a phase shifter or a linear polarizer element incorporated in the optical path of the laser beams before entering the sample chamber. Static and dynamic behavior of dielectric nanoparticles with a refractive index of $n_p = 1.59$ in the interference region of the incident beams is investigated.

In this research, it is assumed that the radius of the particle, a , is much smaller than the incident wavelength, and therefore the dipole (Rayleigh) approximation can be sufficiently accurate to calculate the optical force on the particle and potential energy.²⁴

The scattering forces cancel each other out resulting in a pure conservative gradient force which can be derived from potential energy U as follows²⁵

$$U = -\frac{n_m \alpha}{2c} I, \quad (1)$$

where n_m , c and I are the refractive index of the surrounding medium, the speed of light in a vacuum and the spatial intensity distribution, respectively. The particle polarizability α is given by the Clausius–Mossotti relation²⁴

$$\alpha = 3V \left(\frac{\bar{n}^2 - 1}{\bar{n}^2 + 2} \right), \quad (2)$$

where V and m are the particle volume and relative refractive index of the particle, $\bar{n} = n_p/n_m$, respectively. As can be seen from eqn (1), the potential energy of a very small particle in an optical field is proportional to the light intensity. The optical intensity of a monochromatic wave is proportional to the absolute square of the spatial part of the electric field; $I = (Y/2)|E|^2$, where Y is the admittance of the propagation medium (in our case where the particle is suspended in water $Y = 3.53 \times 10^{-3}$ S). It is convenient to use the notations x_1 , x_2 and x_3 to represent the Cartesian coordinate variables x , y and z , and e_i to denote the unit vector along the positive x_i axis (throughout this paper, x , y and z are equivalent to x_1 , x_2 and x_3). The electric field of the Gaussian beam propagating along the positive x_l axis can be expressed as:

$$\mathbf{E}_l^{(+)} = E_0(w_0/w_l)\exp[-(r_{mn}/w_l)^2]\exp(-i\phi_{lmn})\hat{\mathbf{e}}_m, \quad l, m, n = 1, 2, 3 \text{ and cyclic permutations} \quad (3)$$

where $r_{mn} = \sqrt{x_m^2 + x_n^2}$, $\phi_{lmn} = kx_l + kr_{mn}^2/2R_l - \psi_l$, $w_l = w_0\sqrt{1 + (x_l/z_R)^2}$, $R_l = x_l[1 + (z_R/x_l)^2]$, and $\psi_l = \tan^{-1}(x_l/z_R)$, in which $k = 2\pi/\lambda$ is the wavenumber of the trapping laser in the surrounding medium and $z_R = kw_0^2/2$ is the Rayleigh range. E_0 and w_0 are the electric field amplitude at the beam center and the beam waist radius, respectively.

For the beams propagating along the negative x_l axis, the only change in eqn (3) is $\phi_{lmn} \rightarrow -\phi_{lmn}$. The total optical field can be expressed as the superposition of the individual fields:

$$\mathbf{E} = \sum_{l=1}^3 (\mathbf{E}_l^{(+)} + \mathbf{E}_l^{(-)}) \quad (4)$$

Once the total electric field is determined, the intensity distribution and in turn the potential energy can be computed from eqn (1). For small particles, the trapping stability is strongly affected by the Brownian diffusion of the particle,⁸ and to compare the potential depth with the Brownian thermal energy we normalize the potential energy to the thermal energy of the particle E_T (at room temperature, $E_T = 4.04 \times 10^{-21}$ J).

Results and discussion

Based on the above mathematical formulations, a MATLAB program was written to numerically evaluate the trapping

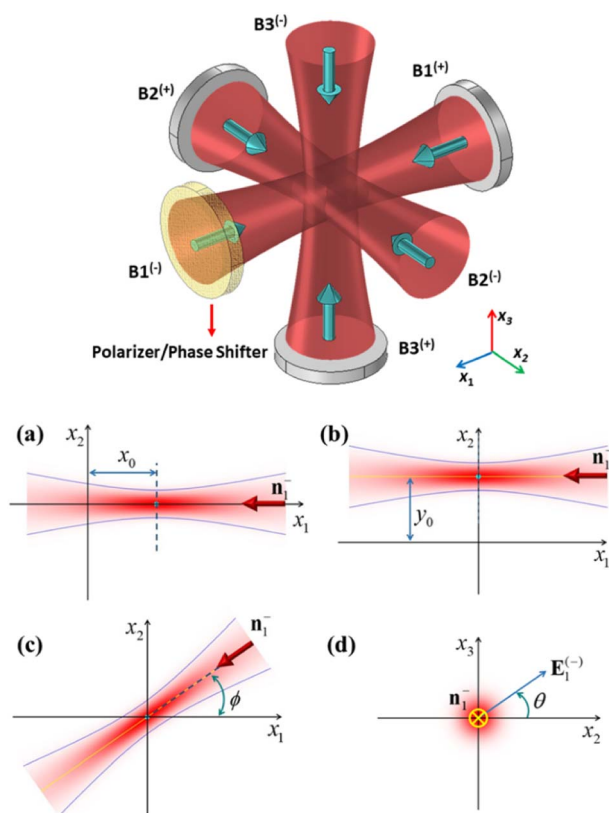


Fig. 1 Schematic diagram of the proposed setup (top diagram) as well as defining the parameters of beam $1^{(-)}$ used in the simulations. (a) Axial offset (x_0), (b) lateral offset (y_0), (c) propagation direction of beam $1^{(-)}$ with respect to the x_1 axis (ϕ), and (d) polarization direction of beam $1^{(-)}$ from the x_2 axis (θ).



properties of the optical lattices created by superimposing three orthogonal Gaussian standing waves. To examine the validity of the MATLAB codes, the simulation codes were run for the specific case of plane waves corresponding to very large values of w_0 . It was observed that as w_0 increases to very large values, the simulation results (not shown) approach the result expected from interfering plane waves, verifying the validity of the MATLAB programs. In the case of interfering plane waves, the generated optical lattices are expected to consist of identical traps (with equal depth) which are exactly centered at the sites of a three-dimensional cubic lattice with a lattice constant of $d = \lambda/2$. For Gaussian beams, there is a small deviation of trap centers from cubic lattice points, and also the central traps have better confinement than peripheral traps. The difference between the Gaussian beam lattices and those of plane waves becomes smaller as the spot size of the interfering Gaussian beams, w_0 , increases. The simulation result for the case of Gaussian beams of spot sizes $w_0 = 4\lambda$ is presented in Fig. 2. This figure shows the normalized potential energy (U/E_T) of the particle in the interference region of the Gaussian beams (see Visualization 1† which shows the iso-surface of the normalized potential energy from different viewpoints). To provide a better understanding of the trapping properties of optical lattices, a two-dimensional view of the normalized potential energy and corresponding optical force is presented in Fig. 3.

A dynamic control over the constructed lattices can be achieved by changing the parameters of the incident beams such as the beam phase. Here we focus on the effects of changing the properties of only one of the interfering beams, namely beam 1⁽⁻⁾ (the beam propagating in the negative x_1 direction), on the constructed lattices. This means that we do not change two parameters at the same time. Fig. 4 shows how the normalized

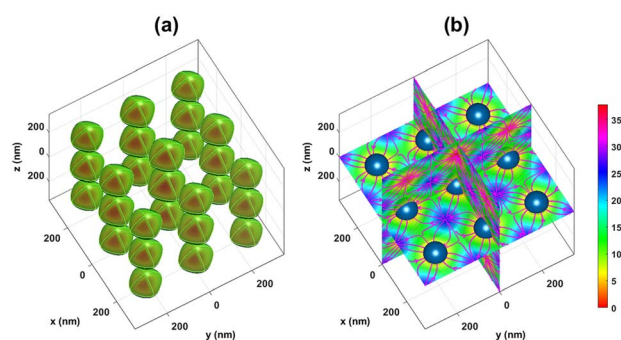


Fig. 2 Normalized potential energy (in $E_T = K_B T$) of a dielectric nanoparticle ($n_p = 1.59$ and $a = 50$ nm) placed in the constructed optical lattices. (a) Iso-surface of the normalized potential energy at an iso-value of 10 as well as the inside structure of the iso-surfaces (slice plots of normalized potential contours). (b) Slice plots of normalized potential energy at three orthogonal slice planes, namely xy , yz and xz planes, as well as the corresponding optical forces (streamlines). The colorbar indicates the normalized potential energy of the particle. The dark blue spheres represent the trapped nanoparticles. The simulation parameters are chosen as: $\lambda_0 = 632.8$ nm, $n_m = 1.33$ (water), and $w_0 = 4\lambda \approx 1.9$ μm and the total incident power is normalized to 1 W ($E_0 \approx 4.1 \times 10^6$ V m⁻¹). The simulation region is a cube with a side of 700 nm. See also Visualization 1† which shows the iso-surface of normalized potential energy from different viewpoints.

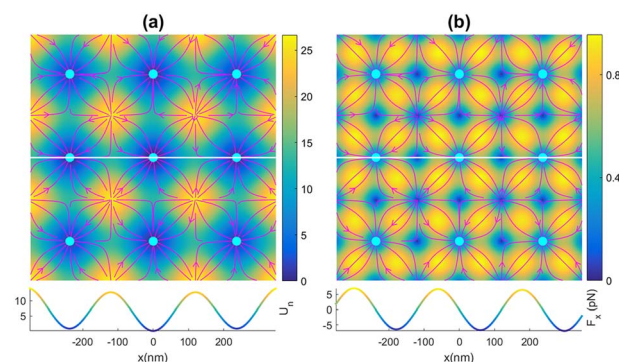


Fig. 3 (a) Top plot: x - y profile of the normalized potential energy of the particle and the corresponding optical force (streamlines). Stable equilibrium points are marked by cyan circles. The colorbar indicates the normalized potential energy of the particle. Bottom plot: normalized potential profile along the white line. (b) Top plot: the magnitude of the optical force in the x - y plane. The colorbar denotes the magnitude of the optical force, $F = \sqrt{F_x^2 + F_y^2}$, in piconewton. Bottom plot: x component of the optical force, $F_x(x)$, along the white line. The simulation parameters are the same as those in Fig. 1.

potential energy of the particle is influenced by changing various parameters of beam 1⁽⁻⁾. Fig. 4a shows a reference result obtained by interfering 3 orthogonal Gaussian standing waves expressed by using eqn (3), corresponding to the case in Fig. 2. It is included only for comparison purposes. Fig. 4b shows the result for the case where the focal plane of beam 1⁽⁻⁾ is shifted in the x_1 direction (axial offset, see panel (a) of Fig. 1) by $x_0 \approx 2.4 \times 10^{-5}$ m. As can be seen from Fig. 4b this axial offset leads to a shift in the interfering lattice along the x_1 direction. Moreover, the depth of traps decreases on increasing the axial offset, especially in the x_1 direction. Therefore, a better confinement can be achieved for the case of zero offset. An ESI video (see visualization 2†) is also provided to demonstrate the evolution of the potential energy with the axial offset. The effects of the lateral offset (a displacement along the direction transverse to the beam axis, see panel (b) of Fig. 1) are shown in Fig. 4c, which correspond to the case where the axis of beam 1⁽⁻⁾ is displaced along the x_2 direction by using $y_0 = w_0 \approx 1.9$ μm . An ESI video (see visualization 3†) is also provided to show how the potential energy evolves with the lateral offset. As can be seen from the numerical results, this lateral offset leads to a decrease in trap depth particularly in the x_1 direction but the change in trap positions is very small. Furthermore, traps situated in the region $x_2 < 0$ exhibit weaker confinement relative to the traps in the region $x_2 > 0$. Fig. 4d shows the trapping potential for the case where the phase of beam 1⁽⁻⁾ is shifted by $\delta = \pi$ rad, i.e. $\phi_{123} \rightarrow \phi_{123} + \pi$. It can be seen that changing the relative phase between beam 1⁽⁺⁾ and beam 1⁽⁻⁾ results in a displacement of the constructed lattices along the x_1 axis. An arbitrary 3D displacement can be achieved by controlling the relative phase between the counterpropagating beams in all three dimensions x_1 , x_2 and x_3 . The displacement of the optical lattices can be exploited for controlled deposition of optically trapped colloidal particles on a surface. Moreover, the trapped particles in these moving lattices can act as nanomotors where



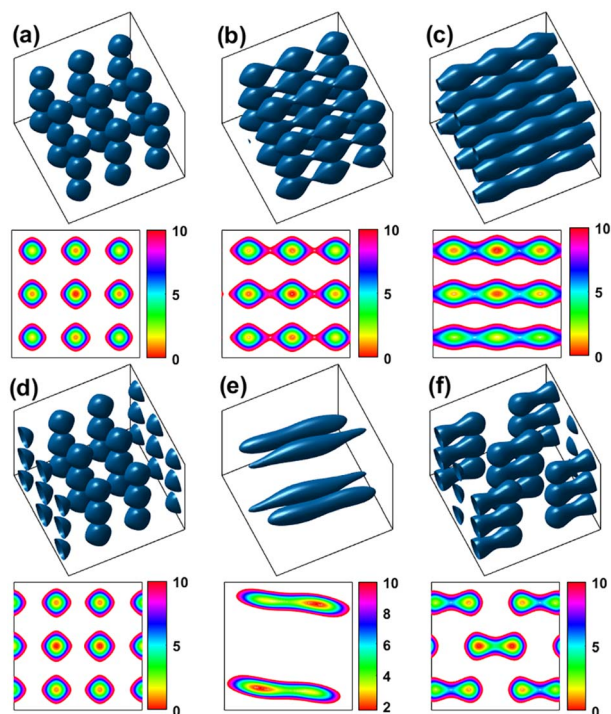


Fig. 4 Influence of changing the beam parameters on the normalized potential energy. The first and third rows show isosurfaces of the normalized potential energy in a 3D view, and the second and fourth rows show the corresponding x - y profiles. (a) Representative reference result obtained by taking the interfering beams exactly the same as those expressed by using eqn (3), corresponding to the case in Fig. 2. (b) Axial offset effects of beam $1^{(-)}$ on the potential landscape: beam $1^{(-)}$ is axially offset by $x_0 = z_R \approx 4 \mu\text{m}$. (c) Lateral offset effects of beam $1^{(-)}$: the beam is laterally offset by $y_0 = w_0 \approx 1.9 \mu\text{m}$ along the x_2 axis. (d) Effects of introducing a phase shift of $\delta = \pi$ rad to beam $1^{(-)}$. (e) Effects of changing the propagation direction of beam $1^{(-)}$ by an angle $\phi = 2\pi/5$ rad along the x_3 axis. (f) Effects of the polarization state of beam $1^{(-)}$ on the potential energy: the polarization vector of beam $1^{(-)}$ is rotated by an angle $\theta = 4\pi/5$ rad along the x_1 axis. The other simulation parameters are the same as in Fig. 2 (see visualizations 2 to 6†).

their movement is controlled by optical force. Reciprocating motion of the trapped particles can also be accomplished by periodically changing the phase of beam $1^{(-)}$. The evolution of the trapping potential with the phase of beam $1^{(-)}$ can be seen in the ESI video (see visualization 4†).

The effect of changing the propagation direction of beam $1^{(-)}$, \mathbf{n}_1^- , on the trapping potential is shown in Fig. 4e. Here, \mathbf{n}_1^- is rotated by an angle $\phi = \pi/4$ around the x_3 axis (ϕ is the counterclockwise angle from the x_1 axis to \mathbf{n}_1^- , see panel (c) of Fig. 1). To provide a better understanding of the behavior of the generated lattices on changing propagation direction ϕ an ESI video (see visualization 5†) is also available. This result is of crucial importance for both micromechanical and microfluidic applications. These produced dynamic optical lattices make it possible to attach two or more colloidal particles together through attractive forces between the particles such as van der Waals forces. This particle attachment can increase the sedimentation rate of a colloidal suspension. These dynamic

lattices also provide a means to control the orientation of non-spherical trapped particles such as nanorods and nanowires. The effects of changing the polarization state of beam $1^{(-)}$ on the trapping potential can be seen in Fig. 4f. Here, the polarization vector of the beam $1^{(-)}$, \mathbf{e}_1^- , is rotated by an angle $\theta = \pi/4$ around the x_1 axis (θ is the counterclockwise angle from the x_2 axis to \mathbf{e}_1^- , see panel (d) of Fig. 1). An ESI video (see visualization 6†) is also provided to visualize the evolution of trapping potential with polarization direction θ . The result obtained in Fig. 4f is highly significant for micro-manipulation applications, and thus needs to be considered again to work on its details.

Fig. 5 shows the effects of changing the polarization direction of beam $1^{(-)}$ on the potential energy of the particle. As can be seen in Fig. 5, as the angle θ increases from $18\pi/25$ to $28\pi/25$, the distance between the two adjacent trapping sites in the interfering region increases from 140 nm to 265 nm, and *vice versa* on decreasing the angle θ from $28\pi/25$ to $18\pi/25$.

These simulation results suggest the possibility of stretching or compressing tethered polymeric molecules such as DNA or actin by adjusting the polarization state of the interfering beams (see Fig. 6 and visualization 7†).

Here, it is assumed that the restoring force exerted by the stretched DNA on the nanobeads has a negligible effect on the position of the trapped beads. Moreover, these generated dynamic lattices can be used to bring colloidal particles into contact and attach them together. The reverse process, particle detachment, can also be achieved using these dynamic lattices (see visualization 6†). It is also possible to control the diffusion of colloidal particles in a suspension using such dynamic lattices. Another important application of these dynamic lattices is found in constructing nanomotors with high controllability. The propulsion mechanism of these light-driven nanomotors is the optical force on nano-objects, and the motion of these nanomotors can be steered along arbitrary trajectories in a simple way. A more flexible dynamic control over the generated lattices can be achieved by adjusting the

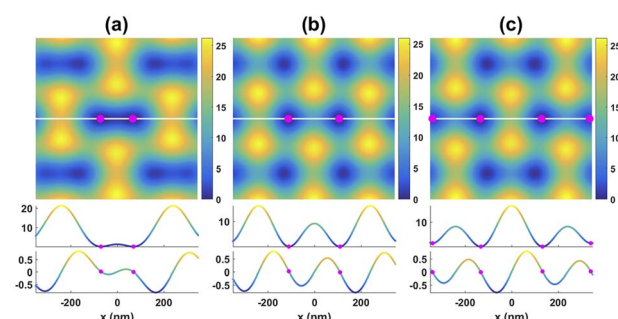


Fig. 5 Potential landscape for three different values of θ to illustrate the effects of the polarization state of the interfering beams on the particle potential. The first row shows the potential profile in the xy plane. The second and third rows show the corresponding potential profiles and x component of the optical force (in piconewtons) along the white line. Parts (a), (b) and (c) correspond to $\theta = 18\pi/25$, $23\pi/25$ and $28\pi/25$ rad, respectively. The magenta circles indicate the potential minima.



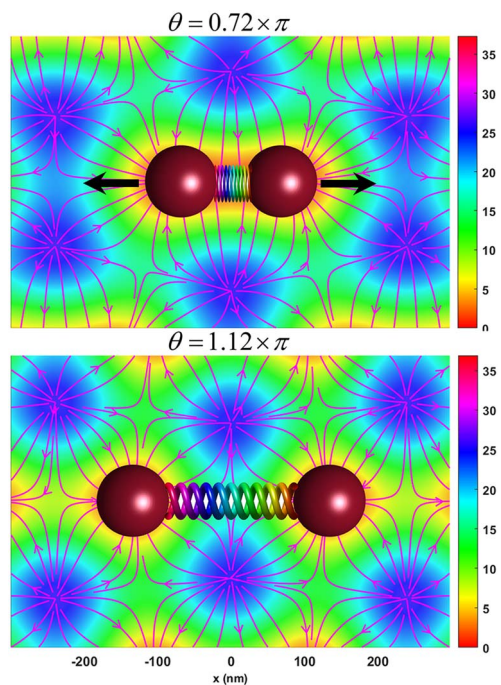


Fig. 6 DNA stretching or compressing with dynamic lattices generated by adjusting the polarization state of beam $1^{(-)}$. The streamlines show the optical force field lines on the xy plane, and the colorbar values indicate normalized potential energy profile in the xy plane. An animation of DNA stretching and compressing is also given in visualization 7.†

parameters of all three negative propagating beams (beam $1^{(-)}$, $2^{(-)}$ and $3^{(-)}$) simultaneously.

It should be mentioned that low index particles can also be stably trapped in these optical lattices, but low index particles are confined around the points of the lowest intensity (see visualization 8†).

The ability to have effective dynamic control over the generated lattices by adjusting the interfering beam parameters opens up many potential applications in various areas of science, particularly in colloidal physics, microfluidics and materials science. We believe that the interference technique has great potential and versatility in the field of optical trapping.

Conclusions

In this work, a simple and effective way to dynamically control 3D optical lattices created by three orthogonal Gaussian standing waves was introduced. The trapping properties of these dynamic lattices for a Rayleigh particle were investigated numerically by writing a MATLAB code based on the dipole approximation. The effects of changing the parameters of only one of the interfering beams on the generated lattices were considered, and the simulation results were presented in both figures and videos. The results showed that the generated lattices can be effectively controlled in a simple way by changing

the beam parameters of one of the incident beams. We believe that the presented results can find profound implications in various areas of the optical trapping field such as colloidal science and biomedical areas.

Conflicts of interest

There are no conflicts to declare.

Notes and references

- H. Wang and M. Pumera, *Chem. Rev.*, 2015, **115**, 8704–8735.
- J. Wang, Z. Xiong, J. Zheng, X. Zhan and J. Tang, *Acc. Chem. Res.*, 2018, **51**, 1957–1965.
- R. Zhuang, D. Zhou, X. Chang, Y. Mo, G. Zhang and L. Li, *Appl. Mater. Today*, 2022, **26**, 101314.
- J. Liu, Z. Huang, H. Yue, R. Zhuang, L. Li, X. Chang and D. Zhou, *Nanoscale*, 2023, **15**, 15831–15839.
- F. Guo, Z. Mao, Y. Chen, Z. Xie, J. P. Lata, P. Li, L. Ren, J. Liu, J. Yang and M. Dao, *Proc. Natl. Acad. Sci. U. S. A.*, 2016, **113**, 1522–1527.
- A. Ozcelik, J. Rufo, F. Guo, Y. Gu, P. Li, J. Lata and T. J. Huang, *Nat. Methods*, 2018, **15**, 1021–1028.
- A. Ohlinger, S. Nedev, A. A. Lutich and J. Feldmann, *Nano Lett.*, 2011, **11**, 1770–1774.
- Z. Liu and D. Zhao, *Opt. Express*, 2012, **20**, 2895–2904.
- K. Onda and F. Arai, *Opt. Express*, 2012, **20**, 3633–3641.
- K. Ladavac, K. Kasza and D. G. Grier, *Phys. Rev. E: Stat., Nonlinear, Soft Matter Phys.*, 2004, **70**, 010901.
- M. Šiler and P. Zemánek, *Opt. Commun.*, 2007, **275**, 409–420.
- D. G. Grier, *Nature*, 2003, **424**, 810–816.
- I. Verdeny, A. Farré, J. Mas Soler, C. López Quesada, E. Martín Badosa and M. Montes Usategui, *Óptica Pura y Aplicada*, 2011, **44**, 527–551.
- K. Dholakia and P. Reece, *Nano Today*, 2006, **1**, 18–27.
- I. Bloch, *Nat. Phys.*, 2005, **1**, 23–30.
- A. Casaburi, G. Pesce, P. Zemánek and A. Sasso, *Opt. Commun.*, 2005, **251**, 393–404.
- F. Nan and Z. Yan, *Adv. Funct. Mater.*, 2019, **29**, 1808258.
- E. Schonbrun, R. Piestun, P. Jordan, J. Cooper, K. D. Wulff, J. Courtial and M. Padgett, *Opt. Express*, 2005, **13**, 3777–3786.
- M. Mohammadnezhad and A. Hassanzadeh, *J. Opt. Soc. Am. B*, 2017, **34**, 983–990.
- M. Mohammadnezhad and A. Hassanzadeh, *J. Nanophotonics*, 2017, **11**, 036007.
- M. Mohammadnezhad, S. R. Saeed and A. Hassanzadeh, *J. Opt.*, 2019, **21**, 105404.
- M. Mohammadnezhad, S. S. Abdulkareem and A. Hassanzadeh, *Opt. Lett.*, 2022, **47**, 4024–4027.
- M. Yevnin, D. Kasimov, Y. Gluckman, Y. Ebenstein and Y. Roichman, *Biomed. Opt. Express*, 2013, **4**, 2087–2094.
- M. Dienerowitz, M. Mazilu and K. Dholakia, *J. Nanophotonics*, 2008, **2**, 021875.
- A. Usman, W.-Y. Chiang and H. Masuhara, *Sci. Prog.*, 2013, **96**, 1–18.

